THE JOURNAL OF PHYSICAL CHEMISTRY C

Article

pubs.acs.org/JPCC

Photon-Assisted CVD Growth of Graphene Using Metal Adatoms As Catalysts

Cheng Gong,[†] Luigi Colombo,*[,‡] and Kyeongjae Cho*[,†]

[†]Department of Materials Science and Engineering, The University of Texas at Dallas, Texas 75080, United States

[‡]Texas Instruments Incorporated, Dallas, Texas 75243, United States

Supporting Information

ABSTRACT: A photon-assisted CVD growth scheme of graphene using metal adatoms as catalysts at the edge of a graphene seed on noncatalytic surfaces, such as silicon dioxide (SiO_2), hexagonal boron nitride (*h*-BN), and graphene, is reported based on first-principles calculations. We systematically examine the possible graphene edge reactions with carbon precursors such as methane, ethylene, or acetylene, using Cu and Ni adatoms as catalysts. The metal atoms adsorbed at the graphene edge capture the ambient ethylene or acetylene molecules, and initiate a series of edge reactions that would be energetically unfavorable in the absence of metal adatoms catalysts. We also suggest that ultraviolet photons can be used to dissociate the stable metal−ethylene or metal−acetylene complex in order to sustain the catalytic reactions. The growth rate of the graphene seed is shown to be slightly higher when on an *h*-BN or graphene substrate. In principle, this process could also be used to heal graphene defects between flakes or improve the continuity of reduced graphene oxide films.

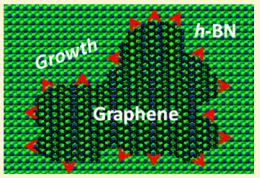

1. INTRODUCTION

Graphene, a monolayer of graphite with two surfaces, is being evaluated for the next generation of nanoelectronic devices for post-CMOS era, among many other applications. In its short history after the successful isolation of graphene, many experimental schemes have been tried to produce large size high-quality graphene sheets. Mechanical exfoliation of graphite[1,2] has been extensively used to obtain graphene with sizes tens of micrometers on the side for all types of measurements. However, this approach is not scalable and will not meet the needs for industrial applications including the electronics industry. It would be desirable to grow graphene on an appropriate substrate by a technique that is more amenable to high volume production, such as chemical vapor deposition (CVD) or other scalable processes. Recently, growth of graphene and multilayer graphene films has been achieved by CVD directly on metal substrates, such as Ir[3] and Cu,[4,5] and also by precipitation from metals, predominantly Ni.[6−8] However, growth of usable large area graphene has only been reproduced uniformly on Cu substrates. The reason for this is associated with the low carbon solubility in Cu versus other metals such as Ni, Co, Pt, Ru, etc.[9,10] Large area graphene has also been grown on Ir; however, iridium's chemical inertness, its high bonding strength with carbon, and its high cost make it an undesirable substrate material.[11,12]

While CVD-grown graphene on Cu can be scaled to any size substrate, it does require transfer from its deposited surface to another more practical surface, usually a dielectric, for it to be used effectively. It would be advantageous to grow graphene directly on a dielectric surface such as amorphous dielectrics, e.g., SiO_2, crystalline high-κ dielectrics or isostructural dielectrics, like hexagonal boron nitride (*h*-BN) or others. The problem is that many dielectric surfaces may not be catalytic. High-κ dielectrics such as MgO,[13,14] ZrO_2,[13] and Co_3O_4[15] have shown the capability for catalyzing the growth of graphene nanoflakes; however, the growth is confined at step edges on (100) surfaces. Although graphene synthesis on monolayer (ML) *h*-BN has been demonstrated recently,[16,17] the effect of ML-Au/bulk-Ni[16] or Ru[17] beneath the ML-BN on the growth of graphene is not well understood, and thus, the catalytic role of the underlying metal cannot be ruled out. The universal ability for growing graphene on an arbitrary dielectric substrate requires introducing a driving force independent of the substrate. So far, there have been rare reports of large area graphene growth directly on noncatalytic surfaces. However, if one were to use a small amount of catalyst on a dielectric surface during the exposure of a carbon precursor, then perhaps one could grow graphene on the dielectric directly.[18,19] Once the metal atoms undertake the role of the catalyst to facilitate the decomposition of carbon-containing molecules such as methane (CH_4), ethylene (C_2H_4), or acetylene (C_2H_2), graphene can be directly grown on any desired dielectric substrate.

We find through a detailed theoretical investigation that metal catalytic adatoms can aid in the dissociation of precursors such as ethylene or acetylene. Then, if one were to use a graphene seed (see Figure 1a,b), then as the metal atoms approach the graphene edge, they react with the carbon precursor leading to dissociation and growth at the graphene edge. However, what we have found is that the strong bonding between the metal and ethylene or metal and acetylene complex immobilizes the metal adatom. In order to overcome

Received: May 30, 2012
Revised: August 6, 2012
Published: August 6, 2012

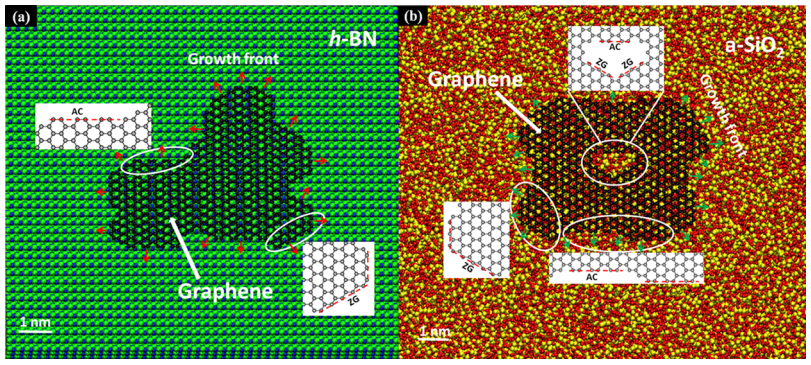

Figure 1. Schematics of a graphene seed on *h*-BN (a) and on amorphous SiO_2 (b) showing armchair and zigzag edges. The areas of the graphene seeds are 17.61 nm^2 (a) and 19.23 nm^2 with a 1.05 nm^2 etch hole (b). Black, green, blue, red, and yellow balls represent C, B, N, O, and Si atoms, respectively. The graphene seed can be grown to a larger size outwardly (a), and the etch hole can be healed by growth inwardly (b).

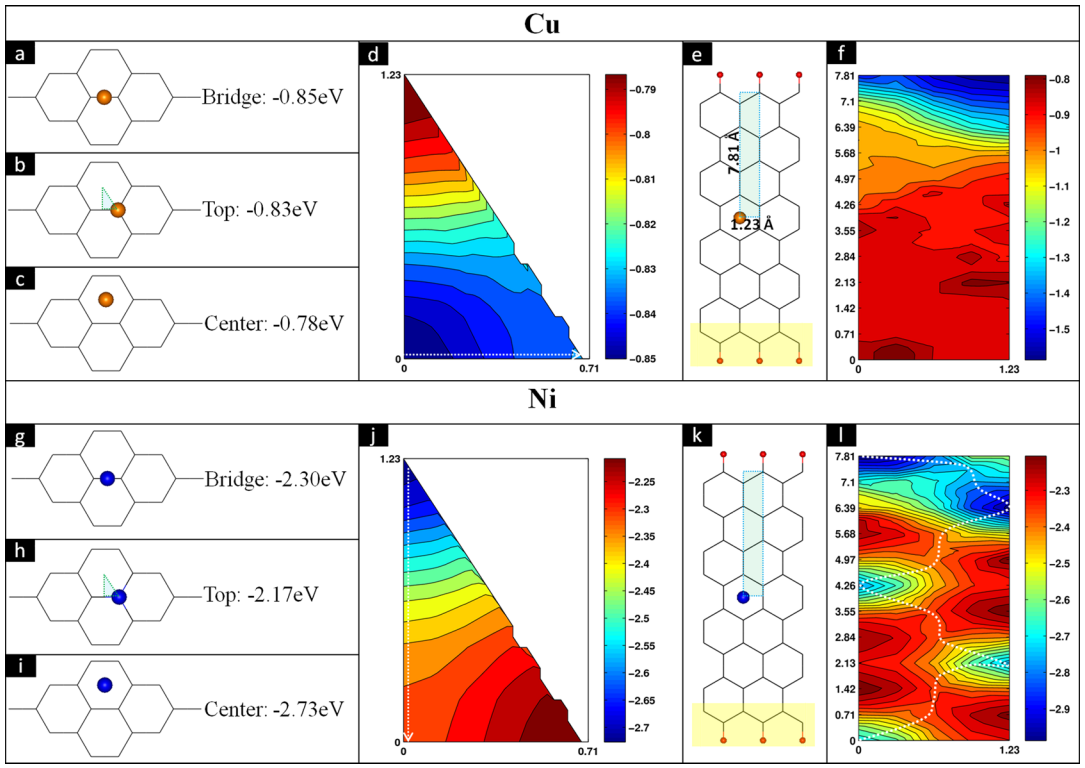

Figure 2. Adsorption energies of Cu and Ni atoms at the edge and inner zones of graphene. Red, blue, and golden balls represent H, Ni, and Cu atoms, respectively. (a,b,c) Cu atom adsorbed above the bridge, top, and center positions of graphene basal plane. (g,h,i) Ni atom adsorbed above the bridge, top, and center positions of graphene basal plane. (d,j) Contour plots of Cu and Ni adsorption above the irreducible triangular zone (Å, shown by green shades in panels b and h) of the graphene basal plane. (f,l) Contour plots for Cu and Ni adsorption above the rectangular zone (Å, shown by green shades in panels e and k) near the zigzag edge of graphene. White dashed lines in panels d, j, and l show the metal atoms' (Cu and Ni) preferential diffusion pathways on the inner zone and edge of graphene. Yellow shaded edges in panels e and k are fixed as bulk, and the other edges are deemed as edge. The unit of the contour bars is eV.

this problem, i.e., catalyst poisoning, we introduced the idea of using ultraviolet (UV) photons to release a metal atom from the complex in order to promote two-dimensional growth. Finally, substrate effects are discussed based on the energy profiles for graphene growth on two representative substrates: ML *h*-BN and ML graphene.

2. THEORETICAL METHODS

In this article, we apply first-principles density functional theory (DFT) calculations to study energetically favorable reaction processes for the growth of graphene. The DFT calculations are performed using the Vienna ab initio simulation package (VASP),[20] where Kohn–Sham single-electron wave functions are expanded by a series of plane waves. The interactions between ions and valence electrons are described by the projector-augmented wave (PAW) method[21] within local density approximation (LDA). The energy cutoff is chosen at 400 eV. Unless specified, all of the calculations are spin-polarized to fully include the edge effects and finite size effects of small atoms and molecules. In the simulated reactions, Ni and Cu atoms are used as catalyst candidates; methane, ethylene, and acetylene are carbon precursor candidates; and zigzag and armchair graphene nanoribbons (GNRs) are used as seeds for the growth along zigzag and armchair edges, as

dx.doi.org/10.1021/jp305268n | J. Phys. Chem. C 2012, 116, 18263–18269

illustrated in Figure 1. We explore a few combinations of these reactants to look for promising growth schemes.

3. RESULTS AND DISCUSSION

3.1. Metal Adatoms' Preferential Adsorption at Graphene Zigzag Edge. To verify the ease with which single metal adatom migrates from the top of the graphene basal plane to the edge, we use a 3 × 3 super cell to calculate the adsorption energies of a metal atom above the irreducible triangle zone defined by three neighboring high symmetry points (bridge, top, and center shown in Figure 2) as apexes and large GNRs to model the edges of the graphene. Super cell 5 × 5 calculations are also tested (see Figure S1 in the Supporting Information). The comparison between 5 × 5 and 3 × 3 super cells shows that a 3 × 3 super cell is enough for the study herein. In the case of the GNR without any underlying substrate, both edges are passivated by hydrogen atoms (Figure 2e,k). The fixed end is considered as bulk graphene, and the other end is relaxed as the edge where catalytically mediated growth occurs. A periodic boundary condition is applied along the edge orientation with 1.2 nm vacuum regions perpendicular to the edge in and out of the graphene basal plane, respectively. Potential catalytic reactions are studied at the relaxed edge. When an infinite substrate (ML *h*-BN or a bottom ML graphene) exists, a larger size substrate super cell is present underneath the graphene seed (i.e., GNR here), so that the possible interaction between GNRs in neighboring super cells is eliminated. The distance between neighboring GNRs in our calculation are larger than 1.6 nm.

Figure 2 shows the adsorption energies of Cu and Ni atoms at the edge and inner zones of graphene and indicates that the adsorption energy difference for the metal adatom on different positions of the graphene basal plane is small. This implies that both Cu and Ni atoms are able to migrate along the graphene basal plane without substantial migration barriers. The white dashed line in Figure 2d shows that a Cu atom migrates along the C−C bond direction with a negligible energy barrier of 0.02 eV, which is further verified by the contour plot in Figure 2f. Although a Ni atom prefers to migrate perpendicularly across the C−C bond with a higher energy barrier of 0.43 eV, this energy barrier is easily overcome by the commonly applied high-temperature processing conditions (~600 °C to ~1050 °C). Compared to the adsorption energies of the metal atoms on top of graphene's basal plane, the more negative adsorption energy at the zigzag edge shows a positional preference for metal atom adsorption (Figures 2f,l), but no strong adsorption preference is observed at the armchair edge (see Figure S2 of the Supporting Information). This observation is consistent with the fact that considerable edge states distribute at the zigzag edge rather than the armchair edge of graphene. Therefore, metal adatoms can migrate on the graphene basal plane with ease and can segregate at the zigzag edge. This segregation phenomenon is in agreement with Choi et al.'s findings.[22] The long-range repulsive interaction[23] is one of the driving forces for metal adatoms spreading rather than forming aggregates. Meanwhile, a relatively low concentration of metal is recommended in the evaluation of this growth process, even at the highest potential growth temperatures, in order to form a sparse distribution of metal adatoms. Once metal adatoms are adsorbed at the zigzag edge, the possibility for edge growth is enhanced.

3.2. Methane As the Carbon Precursor. Since all of the orbitals in the methane molecule are saturated, interatomic interaction between a metal atom and a methane molecule is not expected empirically. If we assume methane could be decomposed and involved into the graphene edge growth, there would be one C−H bond breaking in methane, a second C−H bond breaking at graphene's zigzag edge, one C−C bond formation between the carbon atom of methane and a carbon atom at the graphene edge, and one H−H bond formation within the dissociated H_2 molecule (see Table 1). In order to examine the net energy change after a couple of bond breakings and formations, we performed an ab initio calculation to get the total energy of systems before and after the presumed reaction between methane and the graphene edge. We also calculated the reaction energy for methane decomposition and incorporation at zigzag edge of graphene and found the reaction energy to be too high thus making graphene growth difficult (see Figure S3 in the Supporting Information). This is indirectly supported by experimental data,[4] where the Cu substrate aids in the decomposition of methane into CH_x (x = 1, 2, or 3) radicals[24] before graphene growth.

Table 1. ZGNR Edge Reactions with Methane and Ethylene[a]

graphene edge reactions		
$ZGNR(C_{56}H_{16}) + CH_4 \rightarrow ZGNR{-}CH_3\ (C_{57}H_{18}) + H_2\ (\uparrow)$		
$ZGNR(C_{56}H_{14}) + C_2H_4 \rightarrow ZGNR{-}CH{-}CH_2\ (C_{58}H_{16}) + H_2(\uparrow)$		
calculated bond energy (eV)		
C−H	in CH_4	−5.67
	in C_2H_4	−5.58
	at AGNR edge	−5.57
	at ZCMR edge	−5.63
H−H	in H_2	−4.84
C−C	in graphene	−6.98

[a]Bond energies of C−H, H−H, and C−C bonds in different chemical environments are listed as a reference for an empirical evaluation of the possibility of presumed reactions.

3.3. Ethylene As the Carbon Precursor. Compared with methane, edge reaction using ethylene is more promising considering that (1) the C−H bond in ethylene, which has to be broken, is weaker (−5.58 eV in ethylene versus −5.67 eV in methane, as shown in Table 1) and that (2) the C═C ($\sigma + \pi$) bond between ethylene's carbon atom and graphene's edge carbon atom, which would be formed, is stronger than the pure σ-bond formed for the methane case.

In order to investigate the catalytic role of metal atoms, we performed calculations of comparative groups of growths, in the *absence* (Figure 3a) and *presence* (Figure 3b,c) of metal atoms. In the case where the metal catalyst is absent, edge reaction with ethylene molecules are energetically favorable only in the later stage (the green dashed zone in Figure 3a), as expected based on the above discussions. However, in the first two steps of reactions, there is an energy increase of 0.55 and 0.25 eV for the initial introduction of ethylene molecules (the red dashed zone in Figure 3a). The energy change variations among reactions of different steps can be attributed to the changing localized states of the reaction sites, along with the introduction of the first few ethylene molecules. After the formation of the first few hexagonal rings, the edge reaction is steady with a minor energy drop. The cumulative energy increase of ~0.8 eV in the first two steps (from I to III, Figure 3a) sets a thermodynamic energy barrier, which has to be overcome by introducing an external energy source or be decreased by the introduction of a catalyst in order to promote further reactions

dx.doi.org/10.1021/jp305268n | J. Phys. Chem. C 2012, 116, 18263−18269

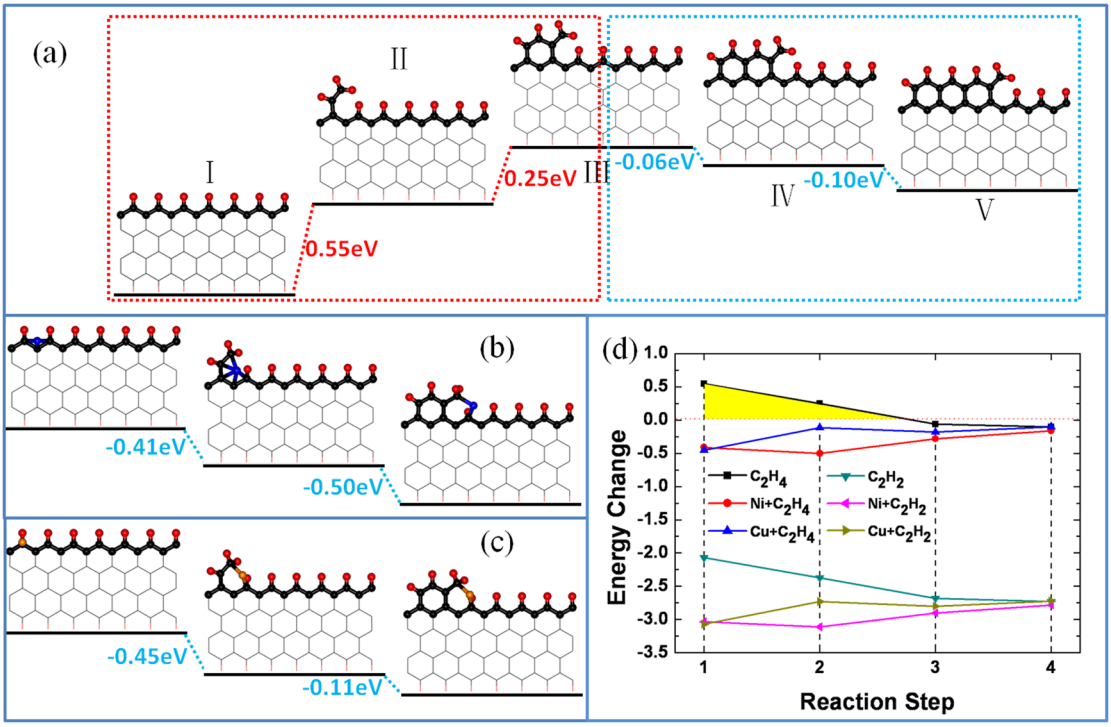

Figure 3. Edge reactions with ethylene in the absence of metal catalysts (a), in the presence of a Ni adatom (b), and in the presence of a Cu adatom (c). (d) Energy change in each initial reaction step for ethylene and acetylene with and without metal adatoms. Energy change (ΔE) in each reaction step is calculated by $\Delta E = (E_{latter} + nE_{H2}) - (E_{former} + E_{CxHy})$, where E_{latter} and E_{former} represent the latter and former structures of each step shown in panels a–c, E_{H2} corresponds to the dissociated H_2 molecule as a reaction product and n = 0, 1, or 2, and E_{CxHy} is for either C_2H_4 or C_2H_2. Black, red, blue, and brown balls represent C, H, Ni, and Cu atoms, respectively.

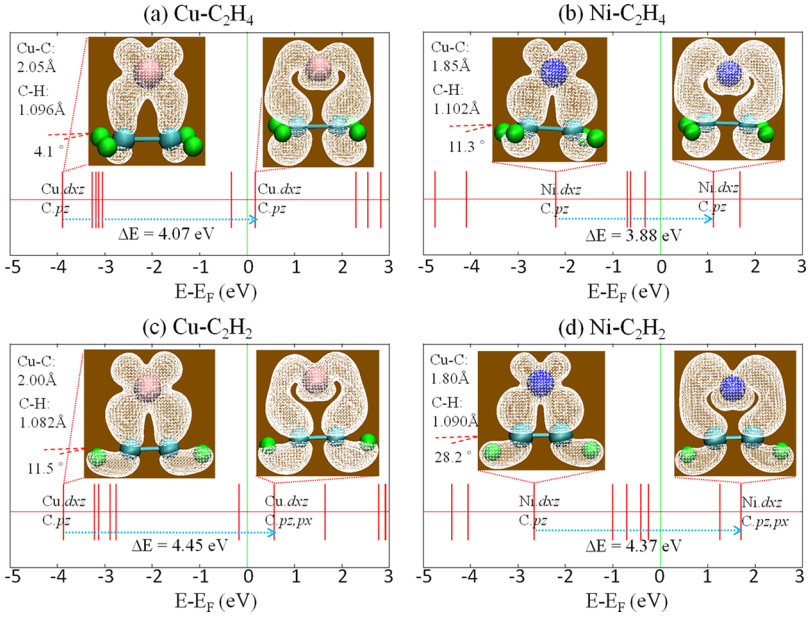

Figure 4. Energy levels in Cu–ethylene (a), Ni–ethylene (b), Cu–acetylene (c), and Ni–acetylene (d) complexes. The cyan, green, pink, and blue balls represent C, H, Cu, and Ni atoms, respectively. The inset configurations show the metal–carbon bonding (left) and antibonding (right) charge distribution contour profiles. Metal–carbon bond lengths, carbon–hydrogen bond lengths, and carbon–hydrogen bond bending angles in the complexes are presented.

and growth. Note that there are kinetic activation barriers between these energy states that make the reaction rates even smaller. The results shown in Figure 3b,c, where Ni and Cu atoms are used as catalysts, show that the metals promote exothermic reactions between the precursor and the edges of the graphene. The higher reactivity is due to the presence of more states of carbon atoms in a newly formed hexagonal ring. Therefore, by using metal atoms at the edges of the graphene, graphene growth is promoted in the absence of a catalytic substrate. In addition to the role of capturing carbon precursor molecules at the edges of the graphene seed, metal atoms play a critical catalytic role (Figure 3), that is, the initiation of a series

dx.doi.org/10.1021/jp305268n | J. Phys. Chem. C 2012, 116, 18263–18269

of edge reactions by decreasing the initial reaction barrier (the yellow shaded zone in Figure 3d).

The interesting difference between Ni and Cu is that Ni can facilitate the second step reaction with a higher energy drop. The difference between the two metals originate from the distinct electronic configurations of Ni ($[Ar]3d^8 4s^2$) and Cu ($[Ar]3d^{10}4s^1$) atoms. A Ni atom has partially occupied *d*-orbitals, which hybridize with carbon atoms more strongly (calculated binding energy (BE) of Ni−C_2H_4 = −3.02 eV, BE of Ni−C_2H_2 = −3.27 eV) than a Cu atom (calculated BE of Cu−C_2H_4 = −1.07 eV and BE of Cu−C_2H_2 = −1.03 eV). A similar conclusion was made on the comparison between Ni−C_2H_4 and Cu−C_2H_4 bonding strength, by Nicolas and Barthelat.[25] After the formation of several rings (4 steps for Cu and a few more steps for Ni), the reaction sites are unchanged with a constant reaction energy drop.

3.4. Acetylene As the Carbon Precursor. Acetylene molecules can be easily involved in edge reactions with a substantial energy drop in each step (see Figure 3d) because of their high reactivity. Acetylene is used to grow graphene at 325 °C on MgO,[13] 480 °C on ZrO_2,[13] and ∼750 °C on ML-*h*-BN/ML-Au/Ni.[16] In ref 26, on Ni foil, graphene growth is achieved at the relatively lower temperature 650−700 °C by using acetylene rather than by using ethylene or methane (both usually ∼1000 °C). The lower temperature implies the higher reactivity of acetylene yielding graphene with low reaction barriers. In the case of acetylene, the main purpose of metal adatoms at the graphene edge is to increase the adsorption efficiency of acetylene molecules at the graphene edges. The metal atoms can also increase the energy drop in the initial reaction steps.

3.5. Prevention of Catalyst Poisoning by UV Activation. The energy diagrams in Figure 3 show that metal atoms at graphene edges can decrease the reaction barriers thus promoting graphene growth at the edges. However, because of the strong bonding between the metal atoms and the hydrocarbon molecules, the metal atom becomes immobilized. We performed simulation to verify the speculation that Cu and Ni atoms bond strongly with incoming ethylene molecules, and the results are shown in Figure 4. In order to enable the metal adatom to continue being an effective catalyst so as to promote continuous growth without incorporation of metals within the graphene, it is necessary to dissociate it from the metal−ethylene or metal−acetylene complexes.

In order to create a feasible strategy to prevent catalyst poisoning, first we should consider the bonding scenarios between metal atoms (Cu and Ni) and the precursor molecules: ethylene and acetylene. It is well-known that there are many configurations of $(metal)_m-(C_2H_4)_n$ (e.g., $Ni(C_2H_4)_n$, n = 2−4;[27] $Ni_m(C_2H_4)_n$;[28] Cu−(C_2H_4);[25] Cr−$(C_2H_4)_6$;[27] $Au^+(C_2H_4)$; and $Pt^+(C_2H_4)$;[29] Ti−C_2H_4−Ti is a high-capacity hydrogen storage media,[30] etc.) with a broad range of applications. However, in our process, the catalytic growth of graphene, metal adatoms pre-exist at the zigzag edges of the graphene seed (refer to Figure 3b,c). When, for example, ethylene is introduced in the reaction chamber, metal−C_2H_4, rather than metal−$(C_2H_4)_n$ (n > 1), are formed at the edges of the graphene seed because the graphene seed blocks the adsorption of a second ethylene molecule to the metal. Therefore, we exclusively studied the structural and electronic properties of four complexes: Cu−C_2H_4, Ni−C_2H_4, Cu−C_2H_2, and Ni−C_2H_2, which are illustrated in Figure 4. As discussed, the ethylene or acetylene bond with Ni is stronger than that with Cu. This is also reflected by the shorter metal−C distances and larger C−H bond bending out of the horizontal molecular plane in Ni cases than that in Cu cases, for both ethylene and acetylene. Meanwhile, there is an interesting change happening to C−H bond lengths in these complexes. The C−H bond length in ethylene (1.102 Å) or acetylene (1.090 Å) in the Ni case is a bit larger than that in the Cu case (1.096 Å in ethylene or 1.082 Å in acetylene). Compared to the Cu−C bond, the Ni−C bond is stronger and weakens the related nearby C−H bonds, and therefore, C−H bond lengths in Ni cases are a little longer than those in Cu. The weakening effect of C−H bonds due to the presence of Ni adsorption suggests a higher catalytic efficiency of Ni than Cu, for the decomposition of these hydrocarbon molecules. Although single metal adatom shows a promise for decomposing hydrocarbon molecules and the corresponding graphene growth, as a catalyst, it has to be released from hydrocarbon molecules for a continuous usage. Photons are commonly used to couple with electrons to excite electrons to antibonding states in order to break chemical bonds. We evaluate first the energy gaps between bonding and antibonding states of the main metal−carbon bond (between C_{pz} and metal d_{xz} orbitals as shown in Figure 4) in metal−ethylene and metal−acetylene complexes. The energy level splittings 4.07 eV (305 nm), 3.88 eV (320 nm), 4.45 eV (279 nm), and 4.37 eV (284 nm) are obtained for Cu−ethylene, Ni−ethylene, Cu−acetylene, and Ni−acetylene complexes, respectively.

Since LDA typically tends to underestimate the energy level splitting,[31] the applied light should be UV with wavelengths shorter than the calculated values. UV lights have already been widely used in various aspects of graphene studies, such as UV-assisted graphene oxide reduction (254 nm in ref 32) and UV spectrometry study of the optical property of graphene (325 nm in ref 33; as deep as ∼200 nm in ref 34). The high transparency of graphene in the UV region demonstrates that the graphene basal plane is marginally affected by UV radiation (as deep as ∼200 nm in ref 35). However, the intensity of UV light needs to be examined experimentally so that the growth efficiency can be optimized without damaging the graphene due to potential overheating. UV radiation has already been successfully used for the photodissociation of metal−ethylene complexes (e.g., 28 800 cm^{-1} (i.e., 3.57 eV) for $Au^+(C_2H_4)$).[28] Upon UV irradiation, electrons are excited from the metal−carbon bond (left inset in Figure 4) to antibonding (right inset in Figure 4), so that the bond is broken. Metal adatoms are released from complexes and migrate to the neighboring edge sites to catalyze the reactions continuously. Cretu et al.[36] have demonstrated that there is a high affinity by the metal adatoms to the defect and strained regions of graphene and expected that the attached metal adatoms have the potential to tailor the properties of graphene. Our work demonstrates a potential engineering route of using attached metal adatoms to catalyze the edge (or etch hole) reaction with carbon precursor molecules to grow or repair the π-network of graphene.

3.6. Substrate Effect. Finally, the substrate effect on the growth of graphene is also studied based on two substrates: ML *h*-BN and ML graphene. Hexagonal BN has the same crystalline structure as graphene, but with a 1.8% larger lattice constant.[37] In our simulations, ML *h*-BN is matched to the graphene lattice (2.46 Å). The calculated equilibrium configuration for *h*-BN/graphene interface has an interface distance of 3.23 Å (experimental value 3.33 Å); half of the carbon atoms are on

dx.doi.org/10.1021/jp305268n | J. Phys. Chem. C 2012, 116, 18263−18269

Table 2. Reaction Energy Profiles of a Bare Graphene Seed and a Graphene Seed on ML-BN and ML-Graphene Substrates, Respectively[a]

		I → II	II → III	III → IV	IV → V
Cu catalyst	bare G	−0.45	−0.11	−0.18	−0.10
	BN (G) substrate	−0.56(−0.57)	−0.18(−0.15)	−0.26(−0.26)	−0.17(−0.16)
Ni catalyst	bare G	−0.41	−0.50	−0.28	−0.16
	BN (G) substrate	−0.46(−0.42)	−0.43(−0.44)	−0.36(−0.35)	−0.20(−0.17)

[a]The Roman numeral indices represent sequential configurations in edge reactions as shown in Figure 3. The reaction energy unit is eV.

top of the boron atoms, and half are on the centers of *h*-BN hexagons (in agreement with ref 38). The graphene seed on a graphene substrate obeys the A−B stacking order with a calculated interface distance 3.3 Å (experimental value 3.34 Å). The simulated structures are schematically shown in Figure S4 of the Supporting Information. In the presence of either substrate, spin-polarization was used in all of the calculations for Ni-catalyzed growth reactions, whereas nonspin-polarization was used for Cu-catalyzed growth reactions. Even in the case of the previous bare graphene seed growth, spin polarized calculations have been shown unnecessary for Cu−adatom related structures (i.e., the structures shown in Figure 3c). Table S1of the Supporting Information shows the detailed comparison between spin-polarized and nonspin-polarized calculations for Cu−adatom related structures, where it is clear that there is a negligible numerical difference.

Graphene on *h*-BN was predicted by first-principles calculations to have a band gap of 53 meV due to the inequivalence of the two carbon sites,[38] whereas experiments found no gap.[39,40] Recent ab initio studies claim that the gap disappears when graphene is misaligned with respect to *h*-BN, which is the likely scenario in realistic devices.[41] Detailed local scanning tunneling spectrometry measurements from Xue et al.[42] show that there is no band gap induced in graphene on *h*-BN, not even locally. The cause is ascribed to a 1.8% lattice mismatch between *h*-BN and graphene and a misalignment between lattices. No clear indicators of electron or hole doping are observed. However, linear π-dispersion of the top layer graphene becomes parabolic because of the coupling to the bottom graphene substrate, without charge transfer between layers. In Table 2, our results show that the energy profiles in catalytic growth reactions change slightly due to the presence of either *h*-BN or graphene substrate. Surprisingly, the changes of the energy profiles due to the two different substrates are almost identical. This can be attributed to their similar negligible substrate effects on the electronic structure of the top graphene seed: neither of these two substrates dopes the top graphene seed or alters its band structure greatly (e.g., gap opening). For other substrates that dope graphene (e.g., SiO_2), the reaction energy for graphene growth may become more negative or positive, depending on the doping type of the graphene (which tunes the zigzag edge states of the graphene seed and thus tunes the edge reactivity). Therefore, we believe that the substrate effects may vary slightly among a variety of weakly coupling noncatalytic dielectric substrates. However, for catalytic dielectrics, the substrate effects are totally different, which is not the intension of this article.

4. CONCLUSIONS

In summary, our calculations show that large area graphene can be grown from graphene seeds by a photon-assisted CVD growth scheme where metal adatoms are used as catalysts and ethylene or acetylene molecules as the carbon sources on noncatalytic dielectric surfaces such as *h*-BN, graphene, SiO_2, etc. The metal adatoms play a dual role, capturing gas molecules from the ambient to the graphene edge and initiating a series of growth reactions. Ultraviolet light is introduced to release metal atoms from the metal−ethylene or metal−acetylene complexes to ensure a continuous catalytic role of the metal adatoms at the edge of the graphene. Noncatalytic weakly coupling substrates, ML *h*-BN and ML-graphene, show little impact to the top graphene seed growth. Photon-assisted CVD using metal adatom catalysts and appropriate hydrocarbon precursors can also be applied to heal graphene defects and create continuous reduced graphene−oxide films.[43]

■ ASSOCIATED CONTENT

Supporting Information

Comparison between 3 × 3 and 5 × 5 graphene supercells for Cu and Ni adatoms adsorptions. Cu and Ni adsorptions on the armchair edge of graphene. Energy profiles for the first CH_4 molecule incorporation into the zigzag edge of graphene. Comparison between spin-polarized and nonspin-polarized calculations of reaction energies for a bare graphene seed growth using a Cu adatom catalyst. Schematics of a graphene seed on ML-BN and ML-graphene. This material is available free of charge via the Internet at http://pubs.acs.org.

■ AUTHOR INFORMATION

Corresponding Author

*E-mail:kjcho@utdallas.edu (K.C.); colombo@ti.com (L.C.).

Notes

The authors declare no competing financial interest.

■ ACKNOWLEDGMENTS

This work was funded by the Nanoelectronic Research Initiative (NRI)−Southwest Academy of Nanotechnology (SWAN). We thank the support from Texas Advanced Computing Center (TACC) for computer resources.

■ REFERENCES

(1) Lu, X. K.; Yu, M. F.; Huang, H.; Ruoff, R. S. *Nanotechnology* **1999**, *10*, 269−272.

(2) Novoselov, K. S.; Geim, A. K.; Morozov, S. V.; Jiang, D.; Zhang, Y.; Dubonos, S. V.; Grigorieva, I. V.; Firsov, A. A. *Science* **2004**, *306*, 666−669.

(3) N'Diaye, A. T.; Bleikamp, S.; Feibelman, P. J.; Michely, T. *Phys. Rev. Lett.* **2006**, *97*, 215501.

(4) Li, X.; Cai, W.; An, J. H.; Kim, S.; Nah, J.; Yang, D.; Piner, R.; Velamakanni, A.; Jung, I.; Tutuc, E.; et al. *Science* **2009**, *324*, 1312−1314.

(5) Bae, S.; Kim, H.; Lee, Y.; Xu, X.; Park, J.-S.; Zheng, Y.; Balakrishnan, J.; Lei, T.; Kim, H. R.; Song, Y., II; et al. *Nat. Nanotechnol.* **2010**, *5*, 574−578.

(6) Yu, Q.; Lian, J.; Siriponglert, S.; Li, H.; Chen, Y. P.; Pei, S.-S. *Appl. Phys. Lett.* **2008**, *93*, 113103.

(7) Sutter, P. W.; Flege, J.-I.; Sutter, E. A. *Nat. Mater.* **2008**, *7*, 406−411.
(8) Hamilton, J. C.; Blakely, J. M. *Surf. Sci.* **1980**, *91*, 199−217.
(9) López, G. A.; Mittemeijer, E. J. *Scr. Mater.* **2004**, *51*, 1−5.
(10) Subramanian, P.; Laughlin, D. *Phase Diagrams of Binary Copper Alloys*; ASM International: Materials Park, OH, 1994; Vol. *10*.
(11) Gong, C.; Lee, G.; Shan, B.; Vogel, E. M.; Wallace, R. M.; Cho, K. *J. Appl. Phys.* **2010**, *108*, 123711.
(12) Gong, C.; Hinojos, D.; Wang, W.; Nijem, N.; Shan, B.; Wallace, R. M.; Cho, K.; Chabal, Y. J. *ACS Nano* **2012**, *6*, 5381−5387.
(13) Scott, A.; Dianat, A.; Börrnert, F.; Bachmatiuk, A.; Zhang, S.; Warner, J. H.; Borowiak-Paleń, E.; Knupfer, M.; Büchner, B.; Cuniberti, G.; et al. *Appl. Phys. Lett.* **2011**, *98*, 073110.
(14) Gaddam, S.; Bjelkevig, C.; Ge, S.; Fukutani, K.; Dowben, P. A.; Kelber, J. A. *J. Phys.: Condens. Matter* **2011**, *23*, 072204.
(15) Zhou, M.; Pasquale, F. L.; Dowben, P. A.; Boosalis, A.; Schubert, M.; Darakchieva, V.; Yakimova, R.; Kong, L.; Kelber, J. A. *J. Phys.: Condens. Matter* **2012**, *24*, 072201.
(16) Usachov, D.; Adamchuk, V. K.; Haberer, D.; Grüneis, A.; Sachdev, H.; Preobrajenski, A. B.; Laubschat, C.; Vyalikh, D. V. *Phys. Rev. B* **2010**, *82*, 075415.
(17) Bjelkevig, C.; Mi, Z.; Xiao, J.; Dowben, P. A.; Wang, L.; Mei, W.-N.; Kelber, J. A. *J. Phys.: Condens. Matter* **2010**, *22*, 302002.
(18) Lee, Y. H.; Kim, S. G.; Tománek, D. *Phys. Rev. Lett.* **2007**, *78*, 2393.
(19) Thess, A.; Lee, R.; Nikolaev, P.; Dai, H.; Petit, P.; Robert, J.; Xu, C.; Lee, Y. H.; Kim, S. G.; Rinzler, A. G.; et al. *Science* **1996**, *273*, 483−487.
(20) Kresse, G.; Furthemüller, J. *J. Comput. Mater. Sci.* **1996**, *6*, 15−50.
(21) Blöchl, P. *Phys. Rev. B: Condens. Matter Mater. Phys.* **1994**, *50*, 17953−17979.
(22) Choi, S.-M.; Jhi, S.-H. *Phys. Rev. Lett.* **2008**, *101*, 266105.
(23) Binz, S. M.; Hupalo, M.; Liu, X.; Wang, C. Z.; Lu, W.-C.; Thiel, P. A.; Ho, K. M.; Conrad, E. H.; Tringides, M. C. *Phys. Rev. Lett.* **2012**, *109*, 026103.
(24) Zhang, W.; Wu, P.; Li, Z.; Yang, J. *J. Phys. Chem. C* **2011**, *115*, 17782−17787.
(25) Nicolas, G.; Barthelat, J. C. *J. Phys. Chem.* **1986**, *90*, 2870−2877.
(26) Nandamuri, G.; Roumimov, S.; Solanki, R. *Nanotechnology* **2010**, *21*, 145604.
(27) Rösch, N.; Hoffmann, R. *Inorg. Chem.* **1974**, *13*, 2656−2666.
(28) Ozin, G.; Power, W.; Upton, T.; Goddard, W. A., III. *J. Am. Chem. Soc.* **1978**, *100*, 4750−4760.
(29) Stringer, K. L.; Citir, M.; Metz, R. B. *J. Phys. Chem. A* **2004**, *108*, 6996−7002.
(30) Durgun, E.; Ciraci, S.; Zhou, W.; Yildirim, T. *Phys. Rev. Lett.* **2006**, *97*, 226102.
(31) Grossman, J. C.; Rohlfing, M.; Mitas, L.; Louie, S. G.; Cohen, M. L. *Phys. Rev. Lett.* **2001**, *86*, 472−475.
(32) Kumar, P.; Subrahmanyam, K. S.; Rao, C. N. R. Graphene Produced by Radiation-Induced Reduction of Graphene Oxide; arXiv:1009.1028, 2010.
(33) Calizo, I.; Bejenari, I.; Rahman, M.; Liu, G.; Balandin, A. A. *J. Appl. Phys.* **2009**, *106*, 043509.
(34) Tang, L.; Ji, R.; Cao, X.; Lin, J.; Jiang, H.; Li, X.; Teng, K. S.; Luk, C. M.; Zeng, S.; Hao, J.; et al. *ACS Nano* **2012**, *6*, 5102−5110.
(35) Weber, C. M.; Eisele, D. M.; Rabe, J. P.; Liang, Y.; Feng, X.; Zhi, L.; Müllen, K.; Lyon, J. L.; Williams, R.; Vanden Bout, D. A.; et al. *Small* **2010**, *6*, 184−189.
(36) Cretu, O.; Krasheninnikov, A. V.; Rodríguez-Manzo, J. A.; Sun, L.; Nieminen, R. M.; Banhart, F. *Phys. Rev. Lett.* **2010**, *105*, 196102.
(37) Liu, L.; Feng, Y. P.; Shen, Z. X. *Phys. Rev. B* **2003**, *68*, 104102.
(38) Giovannetti, G.; Khomyakov, P. A.; Brocks, G.; Kelly, P. J.; van den Brink, J. *Phys. Rev. B* **2007**, *76*, 073103.
(39) Dean, C. R.; Young, A. F.; Meric, I.; Lee, C.; Wang, L.; Sorgenfrei, S.; Watanabe, K.; Taniguchi, T.; Kim, P.; Shepard, K. L.; et al. *Nat. Nanotechnol.* **2010**, *5*, 722−726.
(40) Decker, R.; Wang, Y.; Brar, V. W.; Regan, W.; Tsai, H.-Z.; Wu, Q.; Gannett, W.; Zettl, A.; Crommie, M. F. *Nano Lett.* **2011**, *11*, 2291−2295.
(41) Kharche, N.; Nayak, S. K. *Nano Lett.* **2011**, *11*, 5274−5278.
(42) Xue, J.; Sanchez-Yamagishi, J.; Bulmash, D.; Jacquod, P.; Deshpande, A.; Watanabe, K.; Taniguchi, T.; Jarillo-Herrero, P.; LeRoy, B. J. *Nat. Mater.* **2011**, *10*, 282−285.
(43) Gong, C.; Acik, M.; Abolfath, R. M.; Chabal, Y.; Cho, K. *J. Phys. Chem. C* **2012**, *116*, 9969−9979.